Unimolecular and Bimolecular Calculations for HN_2

P. J. S. B. Caridade, S. P. J. Rodrigues, F. Sousa, and A. J. C. Varandas*

Departamento de Química, Universidade de Coimbra, 3004-535 Coimbra, Portugal

Received: October 27, 2004; In Final Form: December 23, 2004

Using a recently reported double many-body expansion potential energy surface, quasi-classical, statistical mechanics, and quantum resonance calculations have been performed for the HN_2 system by focusing on the determination of bimolecular ($N + NH$ and $H + N_2$) and unimolecular (decomposition of HN_2) rate constants as well as the relevant equilibrium constants.

1. Introduction

It is well established that the hydrodinitrogen radical is an important intermediary species in combustion processes, particularly those concerning the reduction of the NO pollutant.[1−6] It is also relevant in the understanding of noncatalytic radical mechanisms leading to the ammonia production.[7] Although the experimental detection of HN_2 is still to be accomplished (see ref 8), a long-standing conclusion from theoretical methods based on ab initio calculations is that such a species should be metastable with a very short lifetime.[9−11] Despite this, early work[1,2] and even some recent[12] chemical kinetics models of the thermal de-NO_x process (selective noncatalytic reduction of NO by ammonia) assume a large HN_2 lifetime, and hence a small unimolecular decay rate constant, to obtain agreement with existing macroscopic data. By taking into account the predicted theoretical short lifetimes, other researchers[3,5,13,14] have stressed instead the influence of the fast equilibrium $HN_2 \rightleftharpoons H + N_2$ as well as the contribution of reactions not included in the kinetics models. In particular, Dean[15] has pointed out that tweaking critical coefficients to fit macroscopic kinetics data of complex processes always represents a danger. Thus, the inclusion of other relevant molecular processes and use of more accurate data for the involved reactions may help to clarify this issue.

The present work aims to contribute to a better understanding of the title system by studying the relevant unimolecular and bimolecular processes using a recently reported[11] double many-body expansion (DMBE) potential energy surface for the electronic ground state of HN_2. At the bimolecular level, the focus will be on the reaction

$$NH + N \rightarrow H + N_2 \tag{1}$$

and its reverse, which occur adiabatically on such a surface. Reaction 1 plays a key role in the combustion of nitrogen-containing species,[2,16] such as ammonia[17,18] and hydrazine.[14,19] Despite its importance, it has been the subject of only one direct experimental measurement, that by Hack et al.,[20] who reported the rate constant at room temperature, obtained by using a quasi-laser flash photolysis cell. For other temperatures, only crude estimates obtained by indirect means have been suggested.[14,16,19,21] From the perspective of molecular dynamics, the bimolecular reactions considered here have not attracted much attention, partly due to the lack of an accurate global potential energy surface for HN_2. In the present work we will use the quasi-classical trajectory (QCT) method for studying the $N + NH$ reaction over a wide range of temperatures. From this and the equilibrium constant of $NH + N \rightleftharpoons H + N_2$, one may then calculate, assuming micro-reversibility, the rate constant for the endothermic reaction.

The second part of this work focuses on the unimolecular decomposition reaction

$$HN_2 \rightarrow H + N_2 \tag{2}$$

For this, we report calculations of the pure vibrational resonances of HN_2 and an estimate of the thermal high-pressure direct and reverse rate constants for reaction 2. Note that an accurate study of the low-pressure limit is out of the scope of the present work: this would involve a third body (M) and hence the corresponding HN_2M potential energy surface. Bozzelli and Dean[3] estimated such rate constants as the sum of two terms: one provided by the unimolecular decay from the ground vibrational state, and the other, pressure dependent, accounting for collisional vibrational activation where tunneling can also occur. Clearly, a lower bound can be obtained as the decay rate from the lowest vibrational state, which is readily estimated from the resonance calculations. Also of interest for chemical modeling is the equilibrium process

$$HN_2 \rightleftharpoons H + N_2 \tag{3}$$

which is studied by using statistical thermodynamics and the calculated resonances.

The paper is organized as follows. In section 2, we review briefly the DMBE potential energy surface used for the calculations, while sections 3 and 4 are focused on the bimolecular reactions $N + NH$ and $H + N_2$, respectively. The resonance and unimolecular calculations are presented in section 5, while section 6 gathers some final remarks.

2. The HN_2 DMBE Potential Energy Surface

The HN_2 potential energy surface used in the present work has been reported in ref 11 from DMBE[22−24] theory. According to this method, the total interaction potential is first written as a many-body expansion,[25] with every *n*-body term being subsequently split into its (extended) Hartree−Fock (EHF) and dynamical correlation components:

$$V^{(n)} = V^{(n)}_{\mathrm{EHF}} + V^{(n)}_{\mathrm{dc}} \tag{4}$$

* Corresponding author. E-mail: varandas@qtvs1.qui.uc.pt.

10.1021/jp045102g CCC: $30.25
Published on Web 02/17/2005

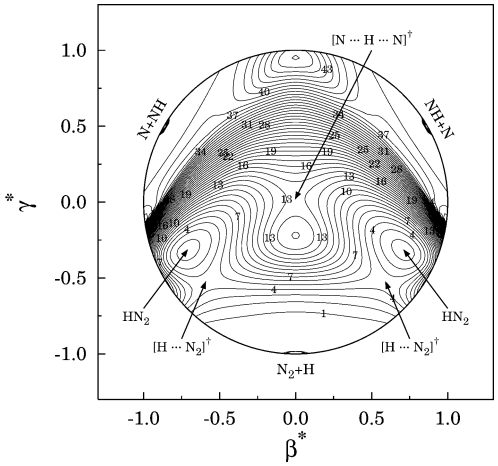

Figure 1. Relaxed triangular plot[29] for the HN_2 DMBE potential energy surface. Contours start at 0.36 E_h and are equally spaced by 6 mE_h.

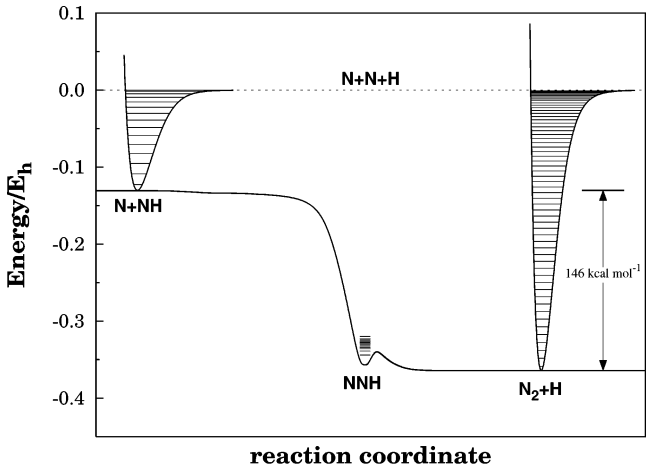

Figure 2. Minimum energy path for the N + NH → N_2 + H reaction.

The various *n*-body dynamical correlation terms are then represented by damped perturbation-type multipolar expansions that account for the dispersion energy at long-range distances. In turn, the EHF terms are written as polynomial × range-determining forms, with the coefficients in them being calibrated from least-squares fits to a total of 972 MRCI[26] energies (based on the aug-cc-pVQZ basis set of Dunning[27]), scaled by the DMBE-SEC[28] method to account for excitations higher than singles and doubles and the incompleteness of the one-electron basis set. The overall root-mean-square deviation (rmsd) over the regions of major chemical interest (up to 40 kcal mol^{-1}) is ≤0.3 kcal mol^{-1}, and hence the DMBE form (discarding the inaccuracies due to not describing seams where electronic states of the same symmetry cross each other) may be judged to be of high accuracy: up to 500 kcal mol^{-1} above the minimum (the rmsd is smaller than 1 kcal mol^{-1}).

Figure 1 shows the DMBE potential energy surface as a relaxed triangular plot[29] using hyperspherical coordinates. The notable features are the two C_s HN_2 equivalent global minima at $\beta^* = \pm 0.714$, $\gamma^* = -0.318$, and the corresponding C_{2v} transition state for isomerization at $\beta^* = 0$, $\gamma^* = 0.026$, which lies 48.44 kcal mol^{-1} above the minima. Also visible are the two saddle points for the HN_2 → N_2 + H unimolecular decomposition, which are located at $\beta^* = \pm 0.593$, $\gamma^* = -0.530$, with the barrier height being 10 kcal mol^{-1} relative to the two equivalent HN_2 metastable minima.

In Figure 2 we show the minimum energy path for the processes studied in the present work. For completeness, the calculated vibrational states of NH, N_2, and N_2H are also indicated to give a general idea of the energetics of the title reactions. Clearly, reaction 1 is highly exothermic (146 kcal mol^{-1}) and of barrierless type. Also visible are the saddle point for the unimolecular dissociation reaction and the metastable character of HN_2.

TABLE 1: Summary of the QCT Results for the N + NH Reaction

		N_2 + H		N + N + H	
T/K	b_{max}/Å	N_r	10^{13} k_1/cm^3 mol^{-1} s^{-1}	N_r	10^{12} k_d/cm^3 mol^{-1} s^{-1}
300	2.7	2657	1.14 ± 0.02		
500	2.7	2648	1.47 ± 0.02		
1000	2.7	2574	2.02 ± 0.03		
2000	2.7	2663	2.96 ± 0.04		
3000	2.7	2701	3.68 ± 0.06		
4000	2.8	2615	4.42 ± 0.07	9	0.15 ± 0.02
5000	2.8	2561	4.84 ± 0.08	34	0.6 ± 0.1
6000	2.9	2504	5.56 ± 0.08	73	1.6 ± 0.2
7000	2.9	2496	5.99 ± 0.08	90	2.2 ± 0.2
10000	2.9	2475	7.1 ± 0.1	277	7.9 ± 0.5
12000	3.0	2250	7.6 ± 0.1	377	12.7 ± 0.6
25000	2.9	2264	10.3 ± 0.2	742	33 ± 1

3. The N + NH Reaction

The use of QCT methods in reaction dynamics has been extensively described in the literature,[30−32] and hence only the details of relevance for the present study will be given. Assuming a thermalized rovibrational distribution for the NH reactant molecule, the rate constant for N_2 + H formation can be determined from the general expression

$$k(T) = g_e\left(\frac{8k_BT}{\pi\mu_{N+NH}}\right)^{1/2}\sum_{vj}\frac{(2j+1)\exp(-E_{vj}/k_BT)}{Q_{vr}(T)} \times \int_0^\infty \frac{E_{tr}}{(k_BT)^2}\exp\left(-\frac{E_{tr}}{k_BT}\right)\sigma(E_{tr},v,j)\,dE_{tr} \quad (5)$$

where $g_e = 1/6$ is the electronic degeneracy factor, k_B the Boltzmann constant, E_{vj} the rovibrational energy of the (v,j) level, Q_{vr} the rovibrational partition function, μ_{N+NH} the reduced mass of the reactants, and $\sigma(E_{tr},v,j)$ the reactive cross section. The translational energy has been obtained by sampling a Maxwell−Boltzmann distribution.[32] In turn, the rovibrational states for each temperature have been sampled using the corresponding cumulative function.[33,34] As in ref 34, we have calculated accurately E_{vj} by solving numerically the Schrödinger equation[35] for the EHFACE2U[36] potential energy curve of NH.[11] Once the (v,j) state is defined for a given trajectory, the internuclear distance is calculated by using the von Newman rejection technique, sampled between the appropriate turning points. Using the Monte Carlo method and the above sampling procedures, eq 5 resumes to calculate

$$k(T) = g_e\left(\frac{8k_BT}{\pi\mu_{N+NH}}\right)^{1/2}\frac{N_r}{N}\pi b_{max}^2 \quad (6)$$

where N_r is the number of reactive trajectories in a batch of N trajectories and b_{max} the maximum impact parameter, which is optimized as described in the literature.[30−32] The 68% error in the rate constant is then given by $\Delta k(T) = k(T)[(N - N_r)/NN_r]^{1/2}$.

Table 1 summarizes the calculated rate constants for the N + NH reaction. The calculations cover the range of temperatures $300 \le T/K \le 25000$, with a total of 3000 trajectories being

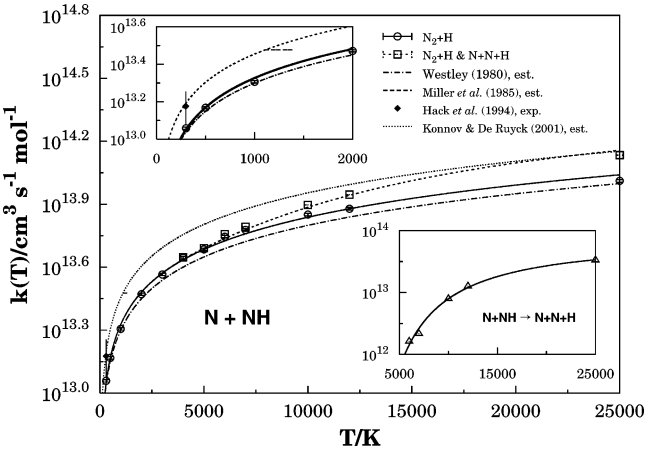

Figure 3. Rate coefficient for the N + NH → N_2 + H reaction as a function of temperature. The open symbols refer to the QCT calculations, while the solid line indicates the Arrhenius fit. Also shown are estimates from various sources,[14,16,21] and the experimental value reported by Hack et al.[20]

integrated for each temperature, which reduces the statistical error to ~1%. Figure 3 shows the calculated rate constant as a function of temperature, and the three-parameter Arrhenius form,

$$k_1 = AT^n \exp(-B/T) \qquad (7)$$

where $A = 6.41 \times 10^{11}$ cm^3 mol^{-1} s^{-1} K^{-n}, $n = 0.51$, and $B = 9.30$ K are the optimum least-squares parameters. As it can be inferred from Figure 3, the employed equal-weight fit mimics well the rate constant over the entire range of temperatures considered in the present work. Perhaps the most salient feature is the strong variation of the rate constant for low and medium temperatures, implying a small influence of the exponential term in eq 7. A similar finding has previously been reported by Westley,[21] who suggested a pure $T^{0.5}$ dependence for the rate constant. Clearly, our result strongly supports his suggestion. Despite its small contribution (and hence an associated large error), we have kept such an exponential term as we expect an anti-threshold behavior for reaction 1 at very high-temperature regimes. In fact, the lower inset in Figure 3 and Table 1 show that the fragmentation channel opens at about 3000 K, although it should be dominant at very high temperatures. It turns out that even at the maximum temperature considered here, such a dissociation channel plays only a minor role, with the corresponding rate constant being about 1 order of magnitude smaller than that yielding N_2 + H. For completeness, the rate constant for collisional induced dissociation has also been fitted to eq 7, the optimum least-squares parameters being $A = 7.57 \times 10^{14}$ cm^3 mol^{-1} s^{-1} K^{-n}, $n = -0.20$, and $B = 27\,254$ K.

Also shown for comparison in Figure 3 (see also the top inset) is the experimental result of Hack et al.,[20] obtained using a quasi-laser flash photolysis cell for low-pressure experiments, $k(298\ \text{K}) = 1.5 \times 10^{13}$ cm^3 mol^{-1} s^{-1}. Such a rate constant has been determined by modeling NH reactant concentrations profiles as a function of the reaction time, with and without N atoms. Our predicted value of 1.1×10^{13} cm^3 mol^{-1} s^{-1} at $T = 298$ K is seen to be lower by only 30%. Unfortunately, the experimental result has not been reported with the associated error bars, although it has been remarked[20] that the major source of error comes from the 20% accuracy of the involved NH(X) calibration. We speculate that a similar error is likely to affect the reported rate constant value, leading to $k(298\ \text{K}) = (1.5 \pm 0.3) \times 10^{13}$ cm^3 mol^{-1} s^{-1}. Clearly, the lower bound approaches our calculated value at room temperature. Besides any other

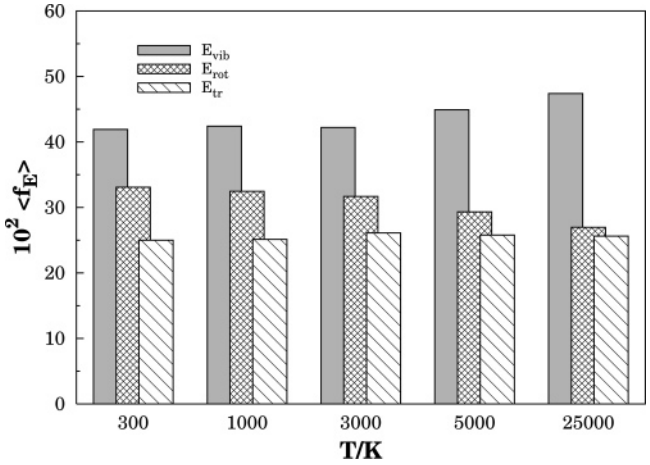

Figure 4. Energy distribution of the product N_2 molecule for five selected temperatures.

unquoted source of experimental error, the difference between the calculated and experimental results may then be attributed to nonadiabatic effects that arise due to the conical intersections that occur for T-shaped and linear configurations of H···N_2.[11] Of course, the use of classical mechanics may itself be a source of error, although the studied temperature range and barrierless character of reaction 1 may suggest that the tunneling effect should not play a significant role in the present work.

Besides the experimental result of Hack et al.,[20] there have been indirect estimates of the rate constant for N_2 + H formation. Westley[21] proposed that such a rate constant should be given by $(6.3 \times 10^{11})T^{0.5}$ cm^3 mol^{-1} s^{-1}, while Miller et al.[16] suggested a temperature-independent rate constant of 3×10^{13} cm^3 mol^{-1} s^{-1} over the interval 1100−1400 K. The most recent analysis comes from the work of Konnov and De Ruyck[14] for the kinetic modeling of the decomposition and flames of hydrazine. Assuming the $T^{0.5}$ dependence proposed by Westley[21] and the value reported by Hack et al.,[20] they suggested the expression $k(T) = (9 \times 10^{11})T^{0.5}$ cm^3 mol^{-1} s^{-1}. At low temperatures, the Westley[21] values are clearly in good agreement with those reported in the present work. The differences become more relevant when comparing with the values recommended by Miller[16] and Konnov and De Ruyck,[14] which are seen to be larger than ours. Interestingly, if one adds the dissociation rate constant (relevant for temperatures higher that 10 000 K) to that of reaction 1, our results become nearly coincident with those of Konnov and De Ruyck[14] at 25 000 K.

We have also analyzed the energy distribution in the products, which shows that the major contribution to be associated with the vibrational degree of freedom (~42−50% of the total energy) of the N_2 molecule. This can be best seen from Figure 4, which shows the fraction of energy release in the products for five selected temperatures. Despite small variations, we may consider the fractions of energy release (translational, rotational, and vibrational) to be nearly constant for low and medium temperatures. For high temperatures (5000 and 25 000 K), the major difference is due to the increase of the fraction of energy released into vibration of N_2 at the expense of a decrease in the rotational part. Another interesting feature is the nearly constant value (25%) of the translational fraction over the entire range of temperatures studied here.

Figure 5 shows the vibrational and rotational distributions of the newly formed N_2 molecules for $T = 300$ K that were obtained from a batch of 50 000 trajectories. The vibrational quantum number has been obtained using the traditional semiclassical method[37] and the N_2 EHFACE2U[36] potential

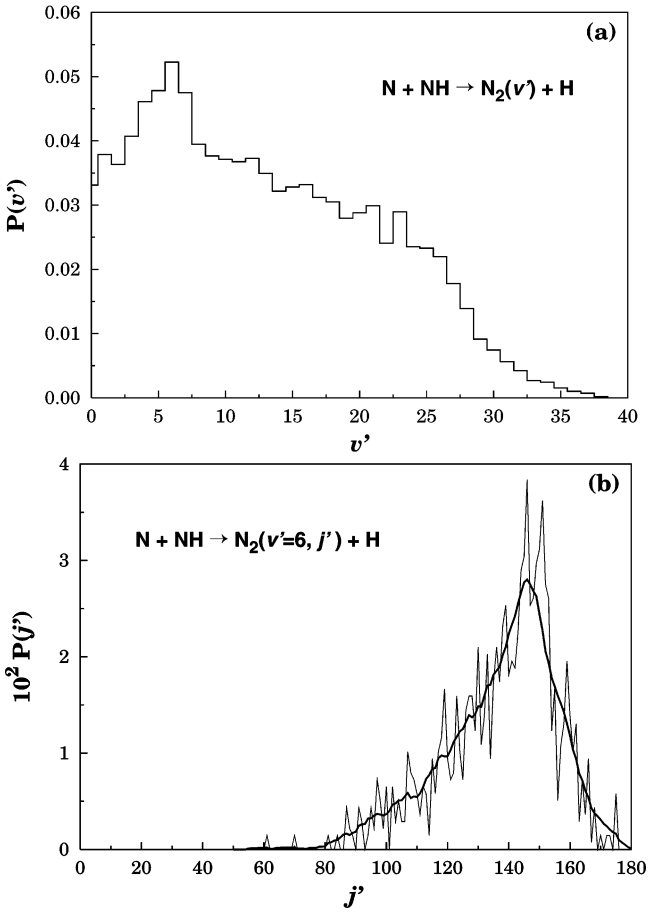

Figure 5. Internal energy distributions of N_2 at $T = 300$ K: (a) vibrational energy; (b) rotational energy for $v' = 6$ (the thick line indicates the smoothed distribution).

energy curve,[11] while the rotational quantum number was calculated from the classical angular momentum, with the assumption of the classical−quantum correspondence. It is seen from panel a that the reaction populates vibrational levels up to $v' = 38$, which is partly due to the high exothermicity of the reaction. Moreover, the maximum population is seen to occur for $v' = 6$. Another significant feature is the broad nature of the distribution up to $v' \approx 26$, which corresponds approximately to the exothermicity of reaction 1. In panel b, we present the rotational distribution corresponding to the vibrational quantum number with maximum population $v' = 6$. Despite the large number of reactive trajectories ($N_r = 26\,425$, corresponding to a probability of 52%), the rotational distribution shows sharp transitions. To smooth them out, we have applied a moving-window averaging technique,[38] which consists of replacing each value by a seven-point average (six to the right and six to the left). As Figure 5b shows, this procedure eliminates such a rough behavior while mimicking the general trends of the rotational distribution. Also visible from the rotational distribution is the fact that the N_2 molecule is formed in highly excited rotational states, following a non-Boltzmann distribution. Recall that for this temperature the fraction of rotational energy release is nearly 35% (Figure 4) of the total energy of the products. A better perspective of the rovibrational distribution is perhaps given by the 3D plot shown in Figure 6 after smoothing the distribution of the rotational degree of freedom. It is seen that the distribution of vibrational and rotational quantum numbers is rather broad, with small populations at low j' states, in a clear manifestation of nonequilibrium.

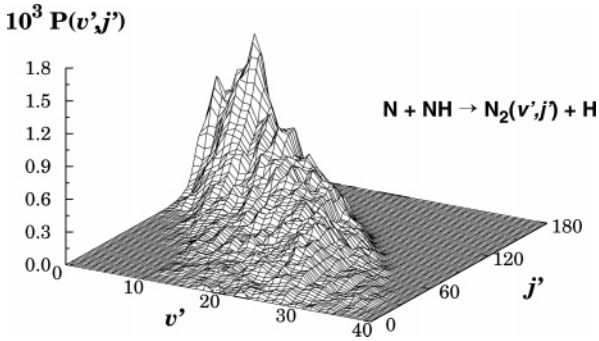

Figure 6. Product rovibrational distribution for N + NH reactive collisions at a temperature of $T = 300$ K.

4. The H + N_2 Reaction

The H + N_2 reaction is highly endothermic, with a very small thermal rate coefficient. Thus, despite the simplicity of the HN_2 DMBE potential energy surface,[11] a study using the QCT method would be extremely time-consuming due to the very small reaction probability at low temperatures. As a result, we have chosen instead to calculate the equilibrium constant for the process $N(^4S) + NH(X\,^3\Sigma^-) \rightleftharpoons N_2(X\,^1\Sigma_g^+) + H(^2S)$ and, by assuming microreversibility, estimate the rate constant for the title reaction by using the rate constant for the reverse reaction calculated in the previous section.

The equilibrium constant for the reaction $N(^4S) + NH(X\,^3\Sigma^-) \rightleftharpoons N_2(X\,^1\Sigma_g^+) + H(^2S)$ assumes the general form

$$K(T) = \frac{Q_{ele}^{H(^2S)}\, Q_{ele}^{N_2(^1\Sigma_g^+)}}{Q_{ele}^{N(^4S)}\, Q_{ele}^{NH(^3\Sigma^-)}}\left(\frac{m_H m_{N_2}}{m_N m_{NH}}\right)^{3/2} \times \frac{\sum_{v,j}^{N_2} n_j(2j+1)\exp(-E_{vj}/k_BT)}{\sum_{v,j}^{NH}(2j+1)\exp(-E_{vj}/k_BT)} \exp\left(-\frac{\Delta E}{k_BT}\right) \quad (8)$$

where $Q_{ele}^{H(^2S)} = 2$, $Q_{ele}^{N_2(^1\Sigma_g^+)} = 1$, $Q_{ele}^{N(^4S)} = 4$, and $Q_{ele}^{NH(^3\Sigma^-)} = 3$ are the electronic partition functions, and E_{vj} denotes in an obvious correspondence the quantum rovibrational energies of N_2 and NH. Note that N_2 has ortho−para nuclear symmetry, which has been accounted by using the factor $n_j = 2/3$ for even j and $n_j = 1/3$ for odd j. Figure 7 shows the calculated equilibrium constant, which has been suitably fitted to eq 7; the optimum least-squares parameters are now $A = 3.48 \times 10^{-2}$ K^{-n}, $n = 0.0062$, and $B = -74\,450$ K. Also shown is the data reported in GRI-Mech 3.0[39] (starting at $T = 2000$ K), which is based on thermodynamical data. Clearly, although covering nearly 8 orders of magnitude, the values obtained from our statistical thermodynamics calculations mimic well the GRI-Mech[39] results. Such a result gives us confidence to extrapolate the parametrized equilibrium constant for medium- and high-temperature regimes, which are more relevant for the H + N_2 process.

From the equilibrium constant, the rate constant for the reverse of reaction 1 may be estimated as $k_{-1} = k_1(T)/K(T)$. Replacing $K(T)$ and $k_1(T)$ by the appropriate expressions yields $A = 1.84 \times 10^{13}$ cm^3 mol^{-1} s^{-1} K^{-n}, $n = 0.50$, and $B = 74\,459$ K. Figure 8 compares the fitted results with those used in GRI-Mech,[39] which are based on their own equilibrium constant and the rate constant reported by Hacket al.[20] for the direct process.

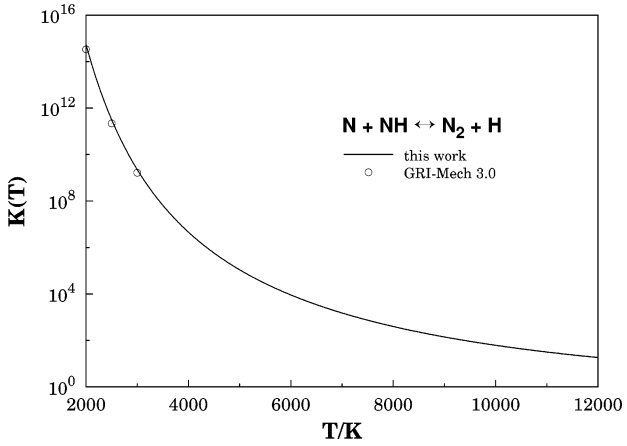

Figure 7. Equilibrium constant for $N(^4S) + NH(X\,^3\Sigma^-) \rightleftharpoons N_2(X\,^1\Sigma_g^+) + H(^2S)$ as a function of temperature.

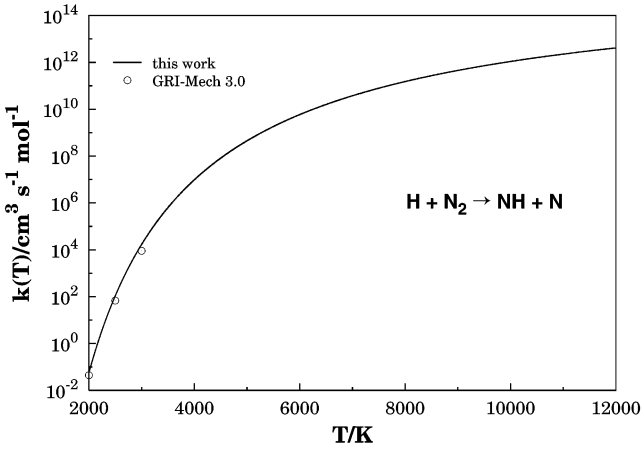

Figure 8. Rate constant as a function of temperature for the $H + N_2$ reaction.

The comparison is fairly good, with a tendency for GRI-Mech[39] to underestimate our results. This trend results from the assumption of an invariance with temperature of the direct reaction between 300 and 3000 K, which is in disagreement with our results and those reported in the literature.[14,16,21]

5. Resonance Energies

A key element for the study of the unimolecular decomposition of HN_2 is the calculation of the resonances energies. In this work, we have calculated them using the stabilization[40−43] and complex[44,45] methods. Such calculations have been performed with the DVR3D suite of programs[46] using Jacobi coordinates (r, R, and θ); r is the N_2 internuclear distance, R the atom center of mass of the diatomic separation, and θ the angle between **R** and **r**. With this definition, one may simplify the computational effort if no energy splitting of the vibrational levels is observed due to isomerization tunneling between the two equivalent minima of HN_2. To check this point, we have performed test calculations in the absence of symmetry and concluded that the energy splitting is negligible. Such a result may be explained on the basis of the high isomerization barrier and shape of the potential energy surface. The primitive DVR basis consisted of $n_r = 40$, $n_R = 65$, $n_\theta = 80$ functions, where the indexes refer to the corresponding coordinates. As parameters for the Morse-like functions,[46] we have chosen $r_e = 2.3a_0$, $D_{e,r} = 0.8E_h$, and $\omega_{e,r} = 0.02E_h$ for the r coordinate, and $R_e = 4.3a_0$, $D_{e,R} = 0.8a_0$, and $\omega_{e,R} = 0.01E_h$ for R. The eigenvalues were obtained via a sequential truncation/diagonalization procedure,[46] with the secular problem being of dimension 3000.

5.1. Stabilization Calculations. According to the stabilization method,[40−43] the resonance states are obtained from the analysis of the eigenvalues of the Hamiltonian when the accessible configurational space is gradually increased. For a natural dissociation coordinate, this can be achieved by varying the size L of the unidimensional box in which the Hamiltonian is diagonalized. Such box sizes have been set equal to the DVR nodes of the R coordinate, varying from $L_{min} = 3.61a_0$ to $L_{max} = 4.56a_0$ and leading to a total of $N = 16$ Hamiltonian diagonalizations. The variation of the density of states is then given by[42]

$$\Delta\rho(E) \simeq -\frac{1}{\Delta L}\sum_j \left(\frac{dE_j(L)}{dL}\right)^{-1}\Bigg|_{E_j(L)=E} - \Delta\rho_0 \qquad (9)$$

where $E_j(L)$ is the energy of the jth level, transformed to a continuous function by interpolation with cubic splines, such that $(dE_j(L)/dL)^{-1}|_{E_j(L)=E} = (dL_j(E)/dE)$ can easily be calculated.[47] Having determined $\Delta\rho(E)$, the spectra of the resonance states can be approximated by Lorentzian functions plus a smooth background, the method being rather sensitive to numerical issues. To circumvent this problem, Madelshtam et al.[42] have shown that the integral of $\Delta\rho(E)$ is an effective phase shift,

$$\Phi(E) - \Phi_0(E) = \pi N(E) + \frac{\pi}{\Delta L}\sum_{j=1}^{N(E)}[L_0 + \Delta L - L_j(E)] \qquad (10)$$

that can then be fitted to a Breit−Wigner function, plus a nonresonant contribution, Φ_b, taken as a smooth low-order polynomial function. One gets

$$\Phi(E) - \Phi_0(E) = \mathrm{atan}\left[\frac{2(E - E_n)}{\Gamma_n}\right] + \Phi_b \qquad (11)$$

where E_n are the resonance energies and Γ_n their widths. The major disadvantage of this method is the large number of box sizes that are required to generate accurate results.[47−49] Since the number of DVR nodes in the present study could not be arbitrarily increased, only the lower resonance states have been estimated (see Table 2).

5.2. Complex Method Calculations. Starting with a square integrable ($\mathcal{L}^2$) basis, the resonant wave functions can be transformed into localized ones by the addition of an asymptotic complex absorbing potential $i\lambda U(R)$. This includes variational parameters for minimizing the reflection and maximizing the absorption of the outgoing wave function.[44,45] Following Skokov et al.[50] and Mussa and Tennyson,[51] we have obtained the resonance parameters from the states of the real Hamiltonian, $\hat{H}$, plus the asymptotic negative imaginary potential (NIP), $\hat{H}' = \hat{H} - i\lambda U(R)$, viz.

$$\hat{H}'\psi_n = \left(E_n - i\frac{\Gamma_n}{2}\right)\psi_n \qquad (12)$$

To represent the NIP (see also refs 52 and 53), we have adopted the form[50,51]

$$U(R) = \left(\frac{R - R_{min}}{R_{max} - R_{min}}\right)^3 \quad R > R_{min} \qquad (13)$$

$$U(R) = 0 \qquad R \le R_{min}$$

TABLE 2: Resonance Parameters for the HN_2 Radical

	DMBE[a]				KSW[b]			
	NIP[c]		stabilization[c]		NIP[c]		Li and Guo[54]	
state	E/cm^{-1}	Γ/cm^{-1}	E/cm^{-1}	Γ/cm^{-1}	E/cm^{-1}	Γ/cm^{-1}	E/cm^{-1}	Γ/cm^{-1}
(000)	4416.3	0.013	4416.3	0.02	4045.4	0.008	4045.17	0.0019
(010)	5500.6	0.16	5500.7	0.19	5115.9	0.04	5115.80	0.034
(001)	6187.5	10.6	6189.3	10	5767.2	2.1	5766.90	2.09
(020)	6573.0	9.6	6573	8	6220.5	1.4	6220.55	1.50
(100)	6713	136			6387.3	56	6386.4	55.8
(011)	7242	34	7238	30	6790.2	8	6789.4	8.18
(030)	7626	44			7289	13	7289.4	13.5
(002)	7962	40			7484	57	7483.0	56.7
(021)	8292	91			7880	33	7879.6	34.6
(040)	8666	99			8309	41	8312.9	42.3
(012)	9011	67			8460	78	8459.2	79.6
(003)	9713	71			9178	93	9174.4	94.6

[a] Potential energy surface from ref 11. [b] Potential energy surface from ref 10. [c] This work.

TABLE 3: Lifetimes and Unimolecular Decay Rates of NH_2

	DMBE[a]		KSW[b]	
state	τ_n/s	k_n/s^{-1}	τ_n/s	k_n/s^{-1}
(000)	4.1(−10)[c]	2.4(9)	2.8(−9)	3.6(8)
(010)	3.3(−11)	3.0(10)	1.6(−10	6.4(9)
(001)	5.0(−13)	2.0(12)	2.5(−12)	3.9(11)
(020)	5.5(−13)	1.8(12)	3.5(−12)	2.8(11)
(100)	3.9(−14)	2.6(13)	9.5(−14)	1.0(13)
(011)	1.6(−13)	6.4(12)	6.5(−13)	1.5(12)

[a] Potential energy surface from ref 11. [b] Potential energy surface from ref 10. [c] The numbers in brackets indicate the power of 10.

As stated in the literature,[44,45,51] the complex method is highly sensitive to the variational parameters in the NIP. We have chosen as optimum values $R_{max} = 6.7a_0$ (taken as the largest R node) and $5.2 \le R_{min}/a_0 \le 5.8$. The energies and widths of the resonances have been obtained as usual from the analysis of λ-trajectories of the complex eigenvalues ($E_n - i\Gamma_n/2$) of $\hat{H}'$. We have considered $0.01 \le \lambda/E_h \le 0.20$ and between 500 and 1000 states for the complex NIP calculations. The resulting resonance parameters for the DMBE and Koizumi et al.[10] (KSW) HN_2 potential energy surfaces based on the larger secular matrices are given in Table 2.

5.3. Resonances, Lifetimes, and Unimolecular Decays. Table 2 compares the calculated resonances and widths obtained by the above two methods with those of Li and Guo[54] based on the KSW[10] potential energy surface using doubled Chebyshev autocorrelation functions. Also shown are the results obtained by applying the complex method to the KSW potential energy surface. Comparing the NIP results with those reported by Li and Guo[54] for the KSW,[10] the differences in energy are seen to be smaller than 2 cm^{-1}, except for the (003) level, where it reaches 4 cm^{-1}. Except for the lowest level, which has a large uncertainty (0.008 ± 0.07), the agreement with the results of Li and Guo[54] on the KSW potential energy surface is good. In comparison with the DMBE potential energy surface,[11] the results show that the energies and widths are generally larger for the latter, which may be attributed to small topographical differences at the regions of the metastable minimum.

For isolated resonances, their lifetimes can be obtained from the associated widths: $\tau_n = \hbar/\Gamma_n$. In turn, the detailed unimolecular decay rate constants can be calculated as $k_n = \Gamma_n/\hbar$. Both quantities are shown in Table 3 using the data obtained from the complex method on the DMBE potential energy surface. As expected from energetic and structural considerations, the lifetimes of the quasibound states of the DMBE potential[11] are smaller than those obtained for the KSW[10] potential.

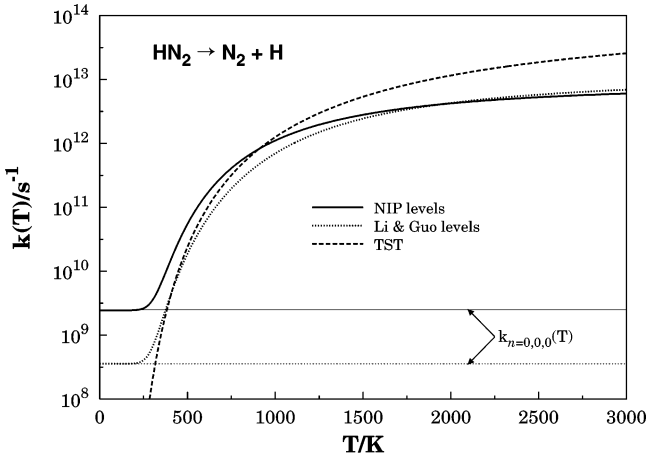

Figure 9. Rate constant as a function of temperature for the $HN_2 \rightarrow H + N_2$ reaction.

The high-pressure limit for the unimolecular rate constant can be estimated from the collision frequency limit.[55,56] One has

$$k(T) = \frac{1}{Q}\sum_n k_n \exp\left(-\frac{\Delta E_n}{k_B T}\right) \tag{14}$$

where Q is the reactants partition function. Figure 9 shows the rate constant calculated from eq 14 using our own unimolecular decay rates as well as those of Li et al.[54] Also shown in this figure is the canonical transition-state theory rate constant and the unimolecular decay of the ground-state vibrational resonance of each potential. The temperature dependence of the rate constant based on the DMBE resonances and widths was fitted to eq 7 in the range 500−3000 K, leading to $A = 1.3 \times 10^{15}$ s^{-1} K^{-n}, $n = -0.53$, and $B = 3404$ K.

Using the equilibrium constant for $HN_2(\tilde{X}\,^2A') \rightleftharpoons N_2(X\,^1\Sigma_g^+) + H(^2S)$, one may obtain the rate constant for the reverse reaction:

$$K(T) = \frac{Q_{ele}^{H(^2S)}\, Q_{ele}^{N_2(^1\Sigma_g^+)}}{Q_{ele}^{HN_2(^2A')}}\left(\frac{m_H m_{N_2}}{m_{HN_2}}\frac{2\pi k_B T}{h^2}\right)^{3/2} V \times \frac{\sum_{v,j}^{N_2} n_j(2j+1)\exp(-E_{vj}/k_B T)}{Q_{vib-rot}^{HN_2}} \exp\left(-\frac{\Delta E}{k_B T}\right) \tag{15}$$

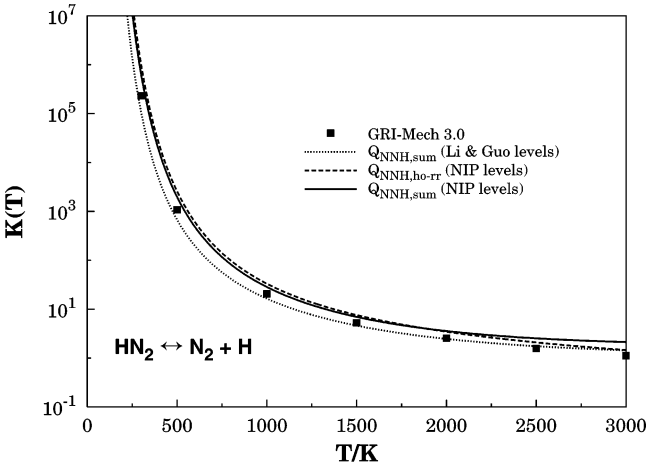

Figure 10. Equilibrium constant for the $HN_2 \rightleftharpoons H + N_2$ process as a function of temperature.

where $Q_{vib-rot}^{HN_2}$ is the rotational−vibrational partition function of HN_2 and V a reference volume (in cm^3); all other quantities have been defined in eq 8. For the calculation of the partition function, we have used two approaches. The first uses the harmonic-oscillator rigid-rotor (ho-rr) model, where

$$Q_{vib-rot}^{HN_2} = \left(\frac{k_B T}{h}\right)^{3/2} \left(\frac{\pi}{A_e B_e C_e}\right)^{1/2} \prod_{i=1}^{3} \frac{\exp(-h\omega_i/k_B T)}{[1 - \exp(-h\omega_i/k_B T)]} \quad (16)$$

with $A_e = 22.353\ cm^{-1}$, $B_e = 1.544\ cm^{-1}$, and $C_e = 1.444\ cm^{-1}$ being the HN_2 rotational constants, and $\omega_1 = 1862\ cm^{-1}$, $\omega_2 = 1086\ cm^{-1}$, and $\omega_3 = 2887\ cm^{-1}$ the harmonic frequencies. The second model uses the partition function

$$Q_{vib-rot}^{HN_2} = \sum_{v,J,K} (2J+1) \exp\left(-\frac{E_{v,J,K}}{k_B T}\right) \quad (17)$$

obtained as a sum over the energy states $E_{v,J,K}$ calculated by using the J-shifting technique,[57] and assuming HN_2 to be a symmetric top with rotational constant $\bar{B}_e = (B_e + C_e)/2$:

$$E_{v,J,K} \simeq E_v^{J=0} + \bar{B}_e J(J+1) + (A_e - \bar{B}_e)K^2 \quad (18)$$

The temperature dependence of the equilibrium constant calculated from the above two models can be expressed using eq 7, leading to $A = 0.24\ K^{-n}$, $n = 0.07$, and $B = -4411$ K for the ho-rr model, and $A = 0.17\ K^{-n}$, $n = 0.11$, and $B = -4312$ K for the sum-over-states one. Such temperature dependences are illustrated in Figure 10, together with the estimate of ref 39. For completeness, we give the parameters in the analytical expression (7) for the reverse of reaction 3: $A = 5.4 \times 10^{15}\ cm^3\ mol^{-1}\ s^{-1}\ K^{-n}$, $n = -0.60$, and $B = 7815$ K for the ho-rr model, and $A = 7.6 \times 10^{15}\ cm^3\ mol^{-1}\ s^{-1}\ K^{-n}$, $n = -0.64$, and $B = 7716$ K for the sum-over-states one. Note that the resonances with very large lifetimes are not expected to be in equilibrium, since they do not form or decay quickly enough to maintain a steady-state requirement.[58] This may not be the case for the decay rates of the HN_2 resonances, which are very short-lived. On the other hand, resonances with very short lifetimes are difficult to distinguish from the so-called nonresonant contributions.[58,59] Thus, our estimated equilibrium constant is likely to underestimates the true one. Using the sum-over-states model with the assumption[57] that the resonances are J-independent leads to the same rate constants within the indicated significant figures. Of course, they are expected to vary with J[60], a point that will not be addressed further in the present work.

6. Final Remarks

We have reported detailed full-dimensional classical and quantum calculations of various rate constants and equilibrium constants pertaining to the title system. Since the potential energy surface used for the calculations has been modeled from accurate MRCI calculations, we believe that such data can be of help in modeling nitrogen chemistry in combustion processes and ammonia production.

Acknowledgment. This work has received financial support from Fundação para a Ciência e Tecnologia (Portugal) under programs POCTI and FEDER. Partial support by the European Community's Human Potential Program under contract HPRN-CT-2002-00170 is also gratefully acknowledged.

Note Added after ASAP Publication. This article was published ASAP on 2/17/2005. A change has been made to an exponent in equation 6. The correct version was posted on 2/18/2005.

References and Notes

(1) Miller, J. A.; Branch, M. C.; Kee, R. J. *Combust. Flame* **1981**, *81*, 43.
(2) Miller, J. A.; Bowman, C. G. *Prog. Energy Combust. Sci.* **1989**, *15*, 287.
(3) Bozzelli, J. W.; Dean, A. M. *Int. J. Chem. Kinet.* **1995**, *27*, 1097.
(4) Hayhurst, A. N.; Hutchinson, E. M. *Combust. Flame* **1998**, *114*, 274.
(5) Hugues, K. J.; Tomlin, A. S.; Hampartsoumian, E.; Zsély, I. G.; vári, M. U.; Turányi, T.; Clague, A. R.; Pilling, M. J. *Combust. Flame* **2001**, *124*, 573.
(6) Tomeczek, J.; Gradoń, B. *Combust. Flame* **1998**, *133*, 311.
(7) Hwang, D.; Mebel, A. M. *J. Phys. Chem. A* **2003**, *107*, 2865.
(8) Selgren, S. F.; McLaughlin, P. W.; Gellene, G. I. *J. Chem. Phys.* **1989**, *90*, 1624.
(9) Walch, S. P.; Duchovic, R. J.; Rohlfing, C. M. *J. Chem. Phys.* **1989**, *90*, 3230.
(10) Koizumi, H.; Schatz, G. C.; Walch, S. P. *J. Chem. Phys.* **1991**, *95*, 4130.
(11) Poveda, L. A.; Varandas, A. J. C. *J. Phys. Chem.* **2003**, *107*, 7923.
(12) Miller, J. A.; Glarborg, P. *Int. J. Chem. Kinet.* **1999**, *31*, 757.
(13) Konnov, A. A.; De Ruyck, J. *Combust. Sci. Technol.* **2001**, *168*, 1.
(14) Konnov, A. A.; De Ruyck, J. *Combust. Flame* **2001**, *124*, 106.
(15) Dean, A. M. *Proceedings of the International Conference on the Foundations of Molecular Modeling and Simulation (FOMMS)*; AIChE Symposium Series 97; American Institute of Chemical Engineers: New York, 2001; p 84.
(16) Miller, J. A.; Branch, M. C.; McLean, W. J.; Chandler, D. W.; Smooke, M. D.; Klee, R. J. *Proceedings of the Combustion Institute, Vol. 20*; The Combustion Institute: Pittsburgh, 1985; p 673.
(17) Kaskan, W. E.; Hughes, D. E. *Combust. Flame* **1973**, *20*, 381.
(18) Skreiberg, O.; Kilpinen, P.; Glarborg, P. *Combust. Flame* **2004**, *136*, 501.
(19) Catoire, L.; Luche, J.; Dupré, G.; Paillard, C. *Shock Waves* **2001**, *11*, 97.
(20) Hack, W.; Wagner, H. G.; Zaspypkin, A. *Ber. Bunsen-Ges. Phys. Chem.* **1994**, *98*, 156.
(21) Westley, F. *Table of recommended rate constants for chemical reactions occuring in combustion;* NBS: Washington, DC, 1980; NSRDS-NBS 67.
(22) Varandas, A. J. C. *Adv. Chem. Phys.* **1988**, *74*, 255.
(23) Varandas, A. J. C. In *Lecture Notes in Chemistry*; Laganá, A., Riganelli, A., Eds.; Springer: Berlin, 2000; Vol. 75, p 33.
(24) Varandas, A. J. C. In *Conical Intersections: Electronic Structure, Dynamics and Spectroscopy*; Yarkony, D., Köppel, H., Domcke, W., Eds.; World Scientific Publishing: Singapore, 2004; Chapter 5.
(25) Murrell, J. N.; Carter, S.; Farantos, S. C.; Huxley, P.; Varandas, A. J. C. *Molecular Potential Energy Functions*; Wiley: Chichester, 1984.
(26) Werner, H.-J.; Knowles, P. J. *J. Chem. Phys.* **1988**, *89*, 5803.
(27) Kendall, R.; Dunning, T., Jr.; Harrison, R. *J. Chem. Phys.* **1992**, *96*, 6769.
(28) Varandas, A. J. C. *J. Chem. Phys.* **1989**, *90*, 4379.
(29) Varandas, A. J. C. *Chem. Phys. Lett.* **1987**, *138*, 455.

(30) Bunker, D. L. *Methods Comput. Phys.* **1971**, *10*, 287.
(31) Porter, R. N.; Raff, L. M. In *Modern Theoretical Chemistry, Dynamics of Molecular Collisions, part B, vol. II*; Miller, W., Ed.; Plenum: New York, 1976; p 1.
(32) Peslherbe, G. H.; Wang, H.; Hase, W. L. *Adv. Chem. Phys.* **1999**, *105*, 171.
(33) Rodrigues, S. P. J.; Varandas, A. J. C. *J. Phys. Chem. A* **2003**, *107*, 5369.
(34) Caridade, P. J. S. B.; Varandas, A. J. C. *J. Phys. Chem. A* **2004**, *108*, 3556.
(35) Leroy, R. J. *LEVEL 7.5, A Computer Program for Solving the Radial Schrödinger Equation for Bound and Quasi-bound Levels*; Chemical Physics Research Report cp-655, University of Waterloo, 2002.
(36) Varandas, A. J. C.; Silva, J. D. *J. Chem. Soc., Faraday Trans.* **1992**, *88*, 941.
(37) Hase, W. L.; Duchovic, R. J.; Hu, X.; Komornik, A.; Lim, K. F.; Lu, D.-H.; Peslherbe, G. H.; Swamy, K. N.; van de Linde, S. R.; Varandas, A. J. C.; Wang, H.; Wolf, R. J. VENUS96. *QCPE Bull.* **1996**, *16*, 43.
(38) Press, W. H.; Teukolski, S. A.; Vetterling, W. T.; Flannery, B. P. *Numerical Recipes in Fortran: the Art of Scientific Computing*; Cambridge University Press: New York, 1992.
(39) Smith, G. P.; Golden, D. M.; Frenklach, M.; Moriarty, N. W.; Eiteneer, B.; Goldenberg, M.; Bowman, C. T.; Hanson, R. K.; Song, S.; Gardiner, W. C., Jr.; Lissianski, V. V.; Qin, Z., http://www.me.berkeley.edu/gri_mech.
(40) Hazi, A. U.; Taylor, H. S. *Phys. Rev. A* **1970**, *1*, 1109.
(41) Mandelshtam, V. A.; Ravuri, T. R.; Taylor, H. S. *Phys. Rev. A* **1993**, *48*, 818.
(42) Mandelshtam, V. A.; Taylor, H. S.; Ryaboy, V.; Moiseyev, N. *Phys. Rev. A* **1994**, *50*, 2764.
(43) Salzgeber, R. F.; Manthe, U.; Weiss, T.; Schlier, C. *Chem. Phys. Lett.* **1996**, *249*, 237.
(44) Jolicard, G.; Austin, E. J. *Chem. Phys.* **1986**, *103*, 295.
(45) Jolicard, G.; Leforestier, C.; Austin, E. J. *J. Chem. Phys.* **1988**, *95*, 1026.
(46) Tennyson, J.; Henderson, J. R.; Fulton, N. G. *Comput. Phys. Commun.* **1995**, *86*, 175.
(47) Ryaboy, V.; Moiseyev, N.; Mandelshtam, V. A.; Taylor, H. S. *J. Chem. Phys.* **1994**, *101*, 5677.
(48) Bludský, O.; Jensen, P. *Mol. Phys.* **1997**, *91*, 653.
(49) Kraemer, W. P.; Spirco, V.; Bludský, O. *Chem. Phys.* **2002**, *276*, 225.
(50) Skokov, S.; Bowman, J. M.; Mandelshtam, V. A. *Phys. Chem. Chem. Phys.* **1999**, *1*, 1279.
(51) Mussa, H. Y.; Tennyson, J. *Chem. Phys. Lett.* **2002**, *366*, 449.
(52) Neuhauser, D.; Baer, M. *J. Chem. Phys.* **1989**, *90*, 4351.
(53) Vibók, A.; Balint-Kurti, G. G. *J. Phys. Chem.* **1992**, *96*, 8712.
(54) Li, G.; Guo, H. *Chem. Phys. Lett.* **2001**, *347*, 443.
(55) Miller, W. H. *J. Phys. Chem.* **1988**, *92*, 4261.
(56) Hase, W. L.; Cho, S.; Lu, D.; Swamy, K. N. *Chem. Phys.* **1989**, *139*, 1.
(57) Bowman, J. M. *J. Phys. Chem. A* **1998**, *102*, 3006.
(58) Roberts, R. E.; Bernstein, R. B.; Curtis, C. F. *J. Chem. Phys.* **1969**, *50*, 5163.
(59) Kendrick, B. K.; Pack, R. *Chem. Phys. Lett.* **1995**, *235*, 291.
(60) Guo, Y.; Thompson, D. L. *J. Chem. Phys.* **2003**, *118*, 3096.